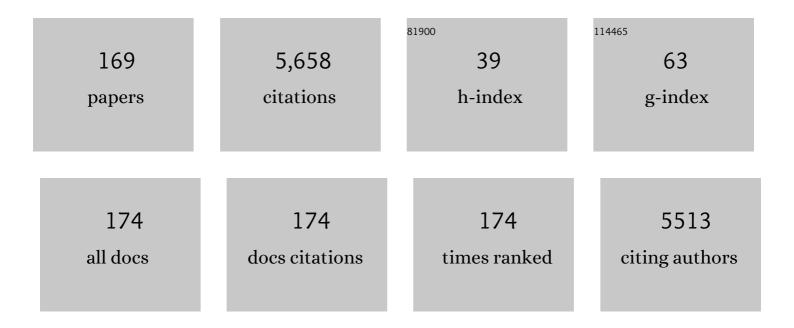
List of Publications by Year in descending order

Source: https://exaly.com/author-pdf/7344344/publications.pdf Version: 2024-02-01



EANLIN

#	Article	IF	CITATIONS
1	Graphene-modified nanosized Ag 3 PO 4 photocatalysts for enhanced visible-light photocatalytic activity and stability. Applied Catalysis B: Environmental, 2015, 162, 196-203.	20.2	298
2	Adsorption and redox reactions of heavy metals on synthesized Mn oxide minerals. Environmental Pollution, 2007, 147, 366-373.	7.5	256
3	Enhanced photocatalytic H2-production activity of C-dots modified g-C3N4/TiO2 nanosheets composites. Journal of Colloid and Interface Science, 2018, 513, 866-876.	9.4	178
4	Sorption behavior of heavy metals on birnessite: Relationship with its Mn average oxidation state and implications for types of sorption sites. Chemical Geology, 2012, 292-293, 25-34.	3.3	157
5	Characteristics of Phosphate Adsorption-Desorption Onto Ferrihydrite. Soil Science, 2013, 178, 1-11.	0.9	155
6	DETERMINATION OF THE POINT-OF-ZERO CHARGE OF MANGANESE OXIDES WITH DIFFERENT METHODS INCLUDING AN IMPROVED SALT TITRATION METHOD. Soil Science, 2008, 173, 277-286.	0.9	123
7	Redox Reactions between Mn(II) and Hexagonal Birnessite Change Its Layer Symmetry. Environmental Science & Technology, 2016, 50, 1750-1758.	10.0	102
8	Mechanisms of Mn(II) catalytic oxidation on ferrihydrite surfaces and the formation of manganese (oxyhydr)oxides. Geochimica Et Cosmochimica Acta, 2017, 211, 79-96.	3.9	100
9	Effects of crystalline phase and morphology on the visible light photocatalytic H ₂ -production activity of CdS nanocrystals. Dalton Transactions, 2014, 43, 7245-7253.	3.3	99
10	Synthesis of Todorokite at Atmospheric Pressure. Chemistry of Materials, 2004, 16, 4330-4336.	6.7	88
11	Adsorption and redox reactions of heavy metals on Fe–Mn nodules from Chinese soils. Journal of Colloid and Interface Science, 2005, 284, 600-605.	9.4	83
12	Characterization of Ni-rich hexagonal birnessite and its geochemical effects on aqueous Pb2+/Zn2+ and As(III). Geochimica Et Cosmochimica Acta, 2012, 93, 47-62.	3.9	83
13	The associations of heavy metals with crystalline iron oxides in the polluted soils around the mining areas in Guangdong Province, China. Chemosphere, 2016, 161, 181-189.	8.2	82
14	Effects of crystallite size on the structure and magnetism of ferrihydrite. Environmental Science: Nano, 2016, 3, 190-202.	4.3	77
15	Relationship Between Pb ²⁺ Adsorption and Average Mn Oxidation State in Synthetic Birnessites. Clays and Clay Minerals, 2009, 57, 513-520.	1.3	71
16	Effects of Fe doping on the structures and properties of hexagonal birnessites – Comparison with Co and Ni doping. Geochimica Et Cosmochimica Acta, 2013, 117, 1-15.	3.9	71
17	Catalytic oxidation of manganese(II) by multicopper oxidase CueO and characterization of the biogenic Mn oxide. Water Research, 2014, 56, 304-313.	11.3	71
18	Characterization of Co-doped birnessites and application for removal of lead and arsenite. Journal of Hazardous Materials, 2011, 188, 341-349.	12.4	70

#	Article	IF	CITATIONS
19	Synthesis of Birnessite from the Oxidation of Mn ²⁺ by O ₂ in Alkali Medium: Effects of Synthesis Conditions. Clays and Clay Minerals, 2004, 52, 240-250.	1.3	68
20	Cadmium Removal from Aqueous Solution by a Deionization Supercapacitor with a Birnessite Electrode. ACS Applied Materials & amp; Interfaces, 2016, 8, 34405-34413.	8.0	67
21	Elemental Composition and Geochemical Characteristics of Iron-Manganese Nodules in Main Soils of China. Pedosphere, 2006, 16, 72-81.	4.0	66
22	Effects of Co and Ni co-doping on the structure and reactivity of hexagonal birnessite. Chemical Geology, 2014, 381, 10-20.	3.3	66
23	Efficient catalytic As(III) oxidation on the surface of ferrihydrite in the presence of aqueous Mn(II). Water Research, 2018, 128, 92-101.	11.3	66
24	Enhanced Dissolution and Transformation of ZnO Nanoparticles: The Role of Inositol Hexakisphosphate. Environmental Science & Technology, 2016, 50, 5651-5660.	10.0	60
25	Cadmium Isotope Fractionation during Adsorption and Substitution with Iron (Oxyhydr)oxides. Environmental Science & Technology, 2021, 55, 11601-11611.	10.0	58
26	The controlling effect of pH on oxidation of Cr(III) by manganese oxide minerals. Journal of Colloid and Interface Science, 2006, 298, 258-266.	9.4	50
27	High-performance Cu2+ adsorption of birnessite using electrochemically controlled redox reactions. Journal of Hazardous Materials, 2018, 354, 107-115.	12.4	50
28	A sol-gel derived pH-responsive bovine serum albumin molecularly imprinted poly(ionic liquids) on the surface of multiwall carbon nanotubes. Analytica Chimica Acta, 2016, 932, 29-40.	5.4	49
29	Co2+-exchange mechanism of birnessite and its application for the removal of Pb2+ and As(III). Journal of Hazardous Materials, 2011, 196, 318-326.	12.4	48
30	Fe-doped cryptomelane synthesized by refluxing at atmosphere: Structure, properties and photocatalytic degradation of phenol. Journal of Hazardous Materials, 2015, 296, 221-229.	12.4	46
31	Influence of Mn(III) availability on the phase transformation from layered buserite to tunnel-structured todorokite. Clays and Clay Minerals, 2008, 56, 397-403.	1.3	45
32	Photochemical Formation and Transformation of Birnessite: Effects of Cations on Micromorphology and Crystal Structure. Environmental Science & amp; Technology, 2018, 52, 6864-6871.	10.0	45
33	Fourier transform infrared spectroscopy study of acid birnessites before and after Pb ²⁺ adsorption. Clay Minerals, 2012, 47, 191-204.	0.6	44
34	Enhancement of Zn2+ and Ni2+ removal performance using a deionization pseudocapacitor with nanostructured birnessite and its carbon nanotube composite electrodes. Chemical Engineering Journal, 2017, 328, 464-473.	12.7	44
35	A Quantitative Model for the Coupled Kinetics of Arsenic Adsorption/Desorption and Oxidation on Manganese Oxides. Environmental Science and Technology Letters, 2018, 5, 175-180.	8.7	44
36	Mechanisms on the morphology variation of hematite crystals by Al substitution: The modification of Fe and O reticular densities. Scientific Reports, 2016, 6, 35960.	3.3	43

#	Article	IF	CITATIONS
37	Adsorption of Cr(VI) on Al-substituted hematites and its reduction and retention in the presence of Fe2+ under conditions similar to subsurface soil environments. Journal of Hazardous Materials, 2020, 390, 122014.	12.4	43
38	Birnessites with Different Average Manganese Oxidation States Synthesized, Characterized, and Transformed to Todorokite at Atmospheric Pressure. Clays and Clay Minerals, 2009, 57, 715-724.	1.3	41
39	Environmental significance of mineral weathering and pedogenesis of loess on the southernmost Loess Plateau, China. Geoderma, 2011, 163, 219-226.	5.1	41
40	Characteristics of micromorphology and element distribution of iron–manganese cutans in typical soils of subtropical China. Geoderma, 2008, 146, 40-47.	5.1	40
41	Rapid determination of the Mn average oxidation state of Mn oxides with a novel two-step colorimetric method. Analytical Methods, 2017, 9, 103-109.	2.7	40
42	Surface Mn(II) oxidation actuated by a multicopper oxidase in a soil bacterium leads to the formation of manganese oxide minerals. Scientific Reports, 2015, 5, 10895.	3.3	39
43	One-step hydrothermal synthesis of LiMn2O4 cathode materials for rechargeable lithium batteries. Solid State Sciences, 2014, 31, 16-23.	3.2	38
44	Photochemical oxidation and dissolution of arsenopyrite in acidic solutions. Geochimica Et Cosmochimica Acta, 2018, 239, 173-185.	3.9	38
45	Transformation of Co-containing birnessite to todorokite: Effect of Co on the transformation and implications for Co mobility. Geochimica Et Cosmochimica Acta, 2019, 246, 21-40.	3.9	38
46	Adsorption (AsIII,V) and oxidation (AsIII) of arsenic by pedogenic Fe–Mn nodules. Geoderma, 2006, 136, 566-572.	5.1	36
47	Transformation of hydroxycarbonate green rust into crystalline iron (hydr)oxides: Influences of reaction conditions and underlying mechanisms. Chemical Geology, 2013, 351, 57-65.	3.3	36
48	Facile synthesis of birnessite-type manganese oxide nanoparticles as supercapacitor electrode materials. Journal of Colloid and Interface Science, 2016, 482, 183-192.	9.4	36
49	Jasmonic Acid-Mediated Aliphatic Glucosinolate Metabolism Is Involved in Clubroot Disease Development in Brassica napus L Frontiers in Plant Science, 2018, 9, 750.	3.6	36
50	Identification and Characterization of <i>Plasmodiophora brassicae</i> Primary Infection Effector Candidates that Suppress or Induce Cell Death in Host and Nonhost Plants. Phytopathology, 2019, 109, 1689-1697.	2.2	36
51	The Presence of Ferrihydrite Promotes Abiotic Formation of Manganese (Oxyhydr)oxides. Soil Science Society of America Journal, 2015, 79, 1297-1305.	2.2	35
52	Molecular-Scale Understanding of Sulfate Exchange from Schwertmannite by Chromate Versus Arsenate. Environmental Science & Technology, 2021, 55, 5857-5867.	10.0	35
53	Pathways of birnessite formation in alkali medium. Science in China Series D: Earth Sciences, 2005, 48, 1438-1451.	0.9	34
54	Solar Irradiation Induced Transformation of Ferrihydrite in the Presence of Aqueous Fe ²⁺ . Environmental Science & Technology, 2019, 53, 8854-8861.	10.0	34

#	Article	IF	CITATIONS
55	Size-dependent sorption of myo-inositol hexakisphosphate and orthophosphate on nano-γ-Al2O3. Journal of Colloid and Interface Science, 2015, 451, 85-92.	9.4	33
56	α-MnO2 nanowires transformed from precursor δ-MnO2 by refluxing under ambient pressure: The key role of pH and growth mechanism. Materials Chemistry and Physics, 2011, 125, 678-685.	4.0	32
57	Influence of vanadium doping on the supercapacitance performance of hexagonal birnessite. Journal of Power Sources, 2015, 277, 26-35.	7.8	32
58	Roles of manganese oxides in degradation of phenol under UV-Vis irradiation: Adsorption, oxidation, and photocatalysis. Journal of Environmental Sciences, 2011, 23, 1904-1910.	6.1	31
59	Characteristics of clay minerals in soil particles of two Alfisols in China. Applied Clay Science, 2016, 120, 51-60.	5.2	31
60	Effects of Al3+ doping on the structure and properties of goethite and its adsorption behavior towards phosphate. Journal of Environmental Sciences, 2016, 45, 18-27.	6.1	31
61	Local structure of Cu2+ in Cu-doped hexagonal turbostratic birnessite and Cu2+ stability under acid treatment. Chemical Geology, 2017, 466, 512-523.	3.3	31
62	Structure and properties of Co-doped cryptomelane and its enhanced removal of Pb 2+ and Cr 3+ from wastewater. Journal of Environmental Sciences, 2015, 34, 77-85.	6.1	30
63	Structure and properties of vanadium(V)-doped hexagonal turbostratic birnessite and its enhanced scavenging of Pb2+ from solutions. Journal of Hazardous Materials, 2015, 288, 80-88.	12.4	30
64	CD-MUSIC-EDL Modeling of Pb ²⁺ Adsorption on Birnessites: Role of Vacant and Edge Sites. Environmental Science & Technology, 2018, 52, 10522-10531.	10.0	30
65	Microstructure, Interaction Mechanisms, and Stability of Binary Systems Containing Goethite and Kaolinite. Soil Science Society of America Journal, 2012, 76, 389-398.	2.2	28
66	Effects of polyphosphates and orthophosphate on the dissolution and transformation of ZnO nanoparticles. Chemosphere, 2017, 176, 255-265.	8.2	28
67	Dissolution and phase transformation processes of hausmannite in acidic aqueous systems under anoxic conditions. Chemical Geology, 2018, 487, 54-62.	3.3	28
68	Formation of Zn-Al layered double hydroxides (LDH) during the interaction of ZnO nanoparticles (NPs) with γ-Al2O3. Science of the Total Environment, 2019, 650, 1980-1987.	8.0	28
69	High Co-doping promotes the transition of birnessite layer symmetry from orthogonal to hexagonal. Chemical Geology, 2015, 410, 12-20.	3.3	27
70	Effects of phosphate and silicate on the transformation of hydroxycarbonate green rust to ferric oxyhydroxides. Geochimica Et Cosmochimica Acta, 2015, 171, 1-14.	3.9	27
71	Effects of Al substitution on local structure and morphology of lepidocrocite and its phosphate adsorption kinetics. Geochimica Et Cosmochimica Acta, 2020, 276, 109-121.	3.9	27
72	Relation of lead adsorption on birnessites with different average oxidation states of manganese and release of Mn2+/H+/K+. Journal of Environmental Sciences, 2009, 21, 520-526.	6.1	26

#	Article	IF	CITATIONS
73	Host Range of <i>Plasmodiophora brassicae</i> on Cruciferous Crops and Weeds in China. Plant Disease, 2016, 100, 933-939.	1.4	26
74	Distinct effects of Al3+ doping on the structure and properties of hexagonal turbostratic birnessite: A comparison with Fe3+ doping. Geochimica Et Cosmochimica Acta, 2017, 208, 268-284.	3.9	26
75	Synthetic Polymer Affinity Ligand for <i>Bacillus thuringiensis</i> (<i>Bt</i>) Cry1Ab/Ac Protein: The Use of Biomimicry Based on the <i>Bt</i> Protein–Insect Receptor Binding Mechanism. Journal of the American Chemical Society, 2018, 140, 6853-6864.	13.7	26
76	Formation of todorokite from "c-disordered―H+-birnessites: the roles of average manganese oxidation state and interlayer cations. Geochemical Transactions, 2015, 16, 8.	0.7	25
77	Putative role of IAA during the early response of Brassica napus L. to Plasmodiophora brassicae. European Journal of Plant Pathology, 2016, 145, 601-613.	1.7	25
78	Influence factors for the oxidation of pyrite by oxygen and birnessite in aqueous systems. Journal of Environmental Sciences, 2016, 45, 164-176.	6.1	25
79	Pb2+ adsorption on birnessite affected by Zn2+ and Mn2+ pretreatments. Journal of Soils and Sediments, 2010, 10, 870-878.	3.0	24
80	Oxidation process of dissolvable sulfide by synthesized todorokite in aqueous systems. Journal of Hazardous Materials, 2015, 290, 106-116.	12.4	24
81	Surface speciation of myo-inositol hexakisphosphate adsorbed on TiO2 nanoparticles and its impact on their colloidal stability in aqueous suspension: A comparative study with orthophosphate. Science of the Total Environment, 2016, 544, 134-142.	8.0	24
82	Self-assembly of birnessite nanoflowers by staged three-dimensional oriented attachment. Environmental Science: Nano, 2017, 4, 1656-1669.	4.3	24
83	Structure and properties of vanadium-doped α-MnO2 and enhanced Pb2+ adsorption phenol/photocatalytic degradation. Materials Chemistry and Physics, 2018, 208, 258-267.	4.0	24
84	Identification and differential expression analysis of anthocyanin biosynthetic genes in leaf color variants of ornamental kale. BMC Genomics, 2019, 20, 564.	2.8	24
85	Synthesis of todorokite-type manganese oxide from Cu-buserite by controlling the pH at atmospheric pressure. Microporous and Mesoporous Materials, 2009, 117, 41-47.	4.4	23
86	Large-scale size-controlled synthesis of cryptomelane-type manganese oxide OMS-2 in lateral and longitudinal directions. Journal of Materials Chemistry, 2011, 21, 5223.	6.7	23
87	Effects of Mn average oxidation state on the oxidation behaviors of As(III) and Cr(III) by vernadite. Applied Geochemistry, 2018, 94, 35-45.	3.0	23
88	Oxidation behavior and kinetics of sulfide by synthesized manganese oxide minerals. Journal of Soils and Sediments, 2011, 11, 1323-1333.	3.0	22
89	Interaction mechanisms and kinetics of ferrous ion and hexagonal birnessite in aqueous systems. Geochemical Transactions, 2015, 16, 16.	0.7	22
90	Facile hydrothermal synthesis and electrochemical properties of orthorhombic LiMnO ₂ cathode materials for rechargeable lithium batteries. RSC Advances, 2014, 4, 13693-13703.	3.6	21

#	Article	IF	CITATIONS
91	Preparation and characterization of biocompatible molecularly imprinted poly(ionic liquid) films on the surface of multi-walled carbon nanotubes. RSC Advances, 2016, 6, 43526-43538.	3.6	21
92	Effects of Reaction Conditions on the Formation of Todorokite at Atmospheric Pressure. Clays and Clay Minerals, 2006, 54, 605-615.	1.3	20
93	Role of Counteranions in Sol–Gel-Derived Alkoxyl-Functionalized Ionic-Liquid-Based Organic–Inorganic Hybrid Coatings for SPME. Chromatographia, 2012, 75, 1421-1433.	1.3	20
94	Desorption ofmyo-inositol hexakisphosphate and phosphate from goethite by different reagents. Journal of Plant Nutrition and Soil Science, 2015, 178, 878-887.	1.9	20
95	The Speciation of Cd in Cd–Fe Coprecipitates: Does Cd Substitute for Fe in Goethite Structure?. ACS Earth and Space Chemistry, 2019, 3, 2225-2236.	2.7	20
96	Transformation of clay minerals in nanoparticles of several zonal soils in China. Journal of Soils and Sediments, 2019, 19, 211-220.	3.0	20
97	The alkaline photo-sulfite system triggers Fe(IV/V) generation at hematite surfaces. Chemical Engineering Journal, 2020, 401, 126124.	12.7	20
98	Composition and transformation of 1.4 nm minerals in cutan and matrix of alfisols in central China. Journal of Soils and Sediments, 2007, 7, 240-246.	3.0	19
99	Synthesis of MnPO4·H2O by refluxing process at atmospheric pressure. Solid State Sciences, 2010, 12, 808-813.	3.2	19
100	THE PROPERTIES OF CLAY MINERALS IN SOIL PARTICLES FROM TWO ULTISOLS, CHINA. Clays and Clay Minerals, 2017, 65, 273-285.	1.3	19
101	The catalytic effect of AQDS as an electron shuttle on Mn(II) oxidation to birnessite on ferrihydrite at circumneutral pH. Geochimica Et Cosmochimica Acta, 2019, 247, 175-190.	3.9	19
102	Cobalt-doped todorokites prepared by refluxing at atmospheric pressure as cathode materials for Li batteries. Electrochimica Acta, 2010, 55, 9157-9165.	5.2	18
103	Formation and Transformation of Iron Oxide–Kaolinite Associations in the Presence of Iron(II). Soil Science Society of America Journal, 2011, 75, 45-55.	2.2	18
104	Zn sorption to biogenic bixbyite-like Mn 2 O 3 produced by Bacillus CUA isolated from soil: XAFS study with constraints on sorption mechanism. Chemical Geology, 2014, 389, 82-90.	3.3	18
105	Zinc removal from aqueous solution using a deionization pseudocapacitor with a high-performance nanostructured birnessite electrode. Environmental Science: Nano, 2017, 4, 811-823.	4.3	18
106	Symbiosis mechanism of iron and manganese oxides in oxic aqueous systems. Chemical Geology, 2018, 488, 162-170.	3.3	18
107	Synthesis of hureaulite by a reflux process at ambient temperature and pressure. Microporous and Mesoporous Materials, 2012, 153, 115-123.	4.4	17
108	Iron-Manganese Nodules Harbor Lower Bacterial Diversity and Greater Proportions of <i>Proteobacteria</i> Compared to Bulk Soils in Four Locations Spanning from North to South China. Geomicrobiology Journal, 2014, 31, 562-577.	2.0	17

#	Article	IF	CITATIONS
109	Facile crystal-structure-controlled synthesis of iron oxides for adsorbents and anode materials of lithium batteries. Materials Chemistry and Physics, 2016, 170, 239-245.	4.0	17
110	Effects of Co(II) ion exchange, Ni(II)- and V(V)-doping on the transformation behaviors of Cr(III) on hexagonal turbostratic birnessite-water interfaces. Environmental Pollution, 2020, 256, 113462.	7.5	17
111	Highly enhanced oxidation of arsenite at the surface of birnessite in the presence of pyrophosphate and the underlying reaction mechanisms. Water Research, 2020, 187, 116420.	11.3	17
112	SnRK1.1â€mediated resistance of <i>Arabidopsis thaliana</i> to clubroot disease is inhibited by the novel <i>Plasmodiophora brassicae</i> effector PBZF1. Molecular Plant Pathology, 2021, 22, 1057-1069.	4.2	17
113	Aging promotes todorokite formation from layered manganese oxide at near-surface conditions. Journal of Soils and Sediments, 2010, 10, 1540-1547.	3.0	16
114	One-step synthesis of sea urchin-like α-MnO2 using KIO4 as the oxidant and its oxidation of arsenite. Materials Letters, 2012, 77, 60-62.	2.6	16
115	Adsorption and precipitation of <i>myo</i> â€inositol hexakisphosphate onto kaolinite. European Journal of Soil Science, 2020, 71, 226-235.	3.9	16
116	Intrinsic mechanisms of calcium sulfite activation by siderite for atrazine degradation. Chemical Engineering Journal, 2021, 426, 131917.	12.7	16
117	Effects of <i>Myo</i> -inositol Hexakisphosphate on Zn(II) Sorption on γ-Alumina: A Mechanistic Study. ACS Earth and Space Chemistry, 2018, 2, 787-796.	2.7	15
118	XAFS studies on surface coordination of Pb2+ on birnessites with different average oxidation states. Colloids and Surfaces A: Physicochemical and Engineering Aspects, 2011, 379, 86-92.	4.7	14
119	Catalytic oxidation of arsenite and reaction pathways on the surface of CuO nanoparticles at a wide range of pHs. Geochemical Transactions, 2018, 19, 12.	0.7	14
120	Effects of Mn ²⁺ , Ni ²⁺ , and Cu ²⁺ on the Formation and Transformation of Hydrosulfate Green Rust: Reaction Processes and Underlying Mechanisms. ACS Earth and Space Chemistry, 2019, 3, 519-530.	2.7	14
121	Preference of Co over Al for substitution of Fe in goethite (α-FeOOH) structure: Mechanism revealed from EXAFS, XPS, DFT and linear free energy correlation model. Chemical Geology, 2020, 532, 119378.	3.3	14
122	Comparing the Infection Biology of Plasmodiophora brassicae in Clubroot Susceptible and Resistant Hosts and Non-hosts. Frontiers in Microbiology, 2020, 11, 507036.	3.5	14
123	Formation and transformation of schwertmannite through direct Fe ³⁺ hydrolysis under various geochemical conditions. Environmental Science: Nano, 2020, 7, 2385-2398.	4.3	14
124	Differences in potassium forms between cutans and adjacent soil matrix in a Grey Clay Soil. Geoderma, 2002, 106, 289-303.	5.1	13
125	Effects of Co and Ni co-doping on the physicochemical properties of cryptomelane and its enhanced performance on photocatalytic degradation of phenol. Materials Chemistry and Physics, 2014, 148, 783-789.	4.0	13
126	Size-controlled synthesis and formation mechanism of manganese oxide OMS-2 nanowires under reflux conditions with KMnO 4 and inorganic acids. Solid State Sciences, 2016, 55, 152-158.	3.2	13

#	Article	IF	CITATIONS
127	Coordination geometry of Zn2+ on hexagonal turbostratic birnessites with different Mn average oxidation states and its stability under acid dissolution. Journal of Environmental Sciences, 2018, 65, 282-292.	6.1	13
128	Genome-wide identification, and phylogenetic and expression profiling analyses of CaM and CML genes in Brassica rapa and Brassica oleracea. Gene, 2018, 677, 232-244.	2.2	13
129	Geochemical characteristics of selected elements in iron–manganese cutans and matrices of Alfisols in central China. Journal of Geochemical Exploration, 2009, 103, 30-36.	3.2	12
130	One-step synthesis of δ-MnO 2 nanoparticles using ascorbic acid and their scavenging properties to Pb(II), Zn(II) and methylene blue. Materials Chemistry and Physics, 2014, 148, 1149-1156.	4.0	12
131	Transformation of the phyllomanganate vernadite to tectomanganates with small tunnel sizes: Favorable geochemical conditions and fate of associated Co. Geochimica Et Cosmochimica Acta, 2021, 295, 224-236.	3.9	12
132	Effect of 1-1 electrolyte concentration on the adsorption/desorption of copper ion on synthetic birnessite. Journal of Soils and Sediments, 2010, 10, 879-885.	3.0	11
133	Synthesis of a Nanofibrous Manganese Oxide Octahedral Molecular Sieve with Co(NH ₃) ₆ ³⁺ Complex Ions as a Template via a Reflux Method. Crystal Growth and Design, 2010, 10, 3355-3362.	3.0	11
134	Effects of myo-inositol hexakisphosphate, ferrihydrite coating, ionic strength and pH on the transport of TiO2 nanoparticles in quartz sand. Environmental Pollution, 2019, 252, 1193-1201.	7.5	11
135	Transformation of Ni-containing birnessite to tectomanganate: Influence and fate of weakly bound Ni(II) species. Geochimica Et Cosmochimica Acta, 2020, 271, 96-115.	3.9	11
136	Factors governing formation of todorokite at atmospheric pressure. Science in China Series D: Earth Sciences, 2005, 48, 1678-1689.	0.9	10
137	Factors Governing the Formation of Lithiophorite at Atmospheric Pressure. Clays and Clay Minerals, 2009, 57, 353-360.	1.3	10
138	ChIP-cloning analysis uncovers centromere-specific retrotransposons in Brassica nigra and reveals their rapid diversification in Brassica allotetraploids. Chromosoma, 2019, 128, 119-131.	2.2	10
139	Coupled morphological and structural evolution of δ-MnO ₂ to α-MnO ₂ through multistage oriented assembly processes: the role of Mn(<scp>iii</scp>). Environmental Science: Nano, 2020, 7, 238-249.	4.3	10
140	Synthesis of todorokite by refluxing process and its primary characteristics. Science in China Series D: Earth Sciences, 2004, 47, 760-768.	0.9	9
141	Effects of Co doping on the structure and physicochemical properties of hausmannite (Mn3O4) and its transformation during aging. Chemical Geology, 2021, 582, 120448.	3.3	9
142	Electrochemical preparation of nanosized manganese dioxides from manganese chloride solutions. Ionics, 2011, 17, 209-216.	2.4	8
143	Oxidation and Catalytic Oxidation of Dissolved Sulfide By Manganite in Aqueous Systems. Clays and Clay Minerals, 2017, 65, 299-309.	1.3	8
144	Effect of Cd and Al Coincorporation on the Structures and Properties of Goethite. ACS Earth and Space Chemistry, 2018, 2, 1283-1293.	2.7	8

#	Article	IF	CITATIONS
145	The preferential retention of VIZn over IVZn on birnessite during dissolution/desorption. Applied Clay Science, 2018, 161, 169-175.	5.2	8
146	Synthesis and Visibleâ€Light Photocatalytic Performance of Cadmium Sulfide and Oxide Hexagonal Nanoplates. ChemPlusChem, 2014, 79, 1726-1732.	2.8	7
147	Absorption mechanisms of Cu2+ on a biogenic bixbyite-like Mn2O3 produced by Bacillus CUA isolated from soil. Geochemical Transactions, 2015, 16, 5.	0.7	6
148	Geochemical Characteristics of Trace Elements in Argillans of Alfisols in Central China. Pedosphere, 2015, 25, 415-427.	4.0	6
149	Interaction mechanism and kinetics of ferrous sulfide and manganese oxides in aqueous system. Journal of Soils and Sediments, 2018, 18, 564-575.	3.0	6
150	Epitaxial growth mechanism of heterogeneous catalytic oxidation of Mn(II) on manganite under oxic conditions. Chemical Geology, 2020, 547, 119670.	3.3	6
151	The distinct effects of isomorphous substitution of various divalence trace metals on hematite structure. Materials Chemistry and Physics, 2018, 217, 40-47.	4.0	5
152	Analysis of Lactobacillus rhamnosus GG in Mulberry Galacto-Oligosaccharide Medium by Comparative Transcriptomics and Metabolomics. Frontiers in Nutrition, 2022, 9, 853271.	3.7	5
153	Effects of cobalt doping on the reactivity of hausmannite for As(III) oxidation and As(V) adsorption. Journal of Environmental Sciences, 2022, 122, 217-226.	6.1	5
154	Facet-dependent adsorption of aluminum(<scp>iii</scp>) on hematite nanocrystals and the influence on mineral transformation. Environmental Science: Nano, 2022, 9, 2073-2085.	4.3	5
155	Characteristics of Iron-Manganese Cutans and Matrices in Alfisols and Ultisols of Subtropical China. Soil Science, 2009, 174, 238-246.	0.9	4
156	Factors Influencing the Elemental Distribution in Iron-Manganese Cutans of Three Subtropical Soils. Soil Science, 2011, 176, 48-56.	0.9	4
157	Transformation from Phyllomanganates to Todorokite under Various Conditions: A Review of Implication for Formation Pathway of Natural Todorokite. ACS Symposium Series, 2015, , 107-134.	0.5	4
158	Marker-free lines of phytase-transgenic Brassica napus show enhanced ability to utilize phytate. Plant Cell, Tissue and Organ Culture, 2020, 140, 11-22.	2.3	4
159	Influences and Mechanisms of As(V) Concentration and Environmental Factors on Hydrosulfate Green Rust Transformation. Acta Chimica Sinica, 2017, 75, 608.	1.4	4
160	Shapeâ€controlled Synthesis of Nanostructure Ramsdelliteâ€type Manganese Oxide at Atmospheric Pressure. Chinese Journal of Chemistry, 2010, 28, 2301-2307.	4.9	3
161	Effect of Cobalt-Doped Framework on Formation of Todorokite from Layered Manganese Oxides with Mg2+/Co2+ Ions as Template. Pedosphere, 2011, 21, 730-737.	4.0	3
162	Comparison of Archaeal Populations in Soil and Their Encapsulated Iron-Manganese Nodules in Four Locations Spanning from North to South China. Geomicrobiology Journal, 2017, 34, 811-822.	2.0	3

#	Article	IF	CITATIONS
163	In situ detection of intermediates from the interaction of dissolved sulfide and manganese oxides with a platinum electrode in aqueous systems. Environmental Chemistry, 2017, 14, 178.	1.5	3
164	Quantitative investigation of ZnO nanoparticle dissolution in the presence of δ-MnO2. Environmental Science and Pollution Research, 2020, 27, 14751-14762.	5.3	3
165	Effect and fate of Ni during aging and thermal-induced phyllomanganate-to-tectomanganate transformation. Geochimica Et Cosmochimica Acta, 2022, 333, 200-215.	3.9	2
166	Microcalorimetric Study on the Growth and Metabolism of a Manganese-Oxidizing Bacterium and its Mutant Strain. Geomicrobiology Journal, 2015, 32, 585-593.	2.0	1
167	The Influence of Zn2+ and Mn2+ on Pb2+ Adsorption Behaviors of Birnessite. , 2010, , 151-153.		1
168	Synthesis of Ramsdellite by Refluxing Process and Its Influencing Factors. Wuji Cailiao Xuebao/Journal of Inorganic Materials, 2011, 26, 321-326.	1.3	0
169	Mechanisms of efficient As(III) and As(V) removal by Ni-coprecipitated hausmannite nanocomposites. Journal of Environmental Chemical Engineering, 2022, 10, 107684.	6.7	ο